Lawrence Berkeley National Laboratory
LBL Publications

Title

Ultrafast Exciton Dynamics of CH3NH3PbBr3 Perovskite Nanoclusters.

Permalink

https://escholarship.org/uc/item/57k9b52f

Authors

Cherrette, Vivien L
Chou, Kai-Chun
Zeitz, David
et al.

Publication Date

2024-05-08

DOI

10.1021/acs.jpclett.4c01203

Ultrafast Exciton Dynamics of CH$_3$NH$_3$PbBr$_3$ Perovskite Nanoclusters

Vivien L. Cherrette[a], Kai-Chun Chou[a], Melissa Guarino-Hotz[a], David Zeitz[a], Mariam Khvichia[a],

Jeremey Barnett[a], Allison Win[a], Finn Babbe[b], and Jin Z. Zhang*[a]

[a]Department of Chemistry and Biochemistry, University of California, Santa Cruz, California

95064, United States

[b]Chemical Science Division, Lawrence Berkeley National Laboratory, Berkeley, California

94720, United States

Corresponding authors: zhang@ucsc.edu (J. Z.)

Abstract

Exciton dynamics of perovskite nanoclusters have been investigated for the first time using femtosecond transient absorption (TA) and time-resolved photoluminescence (TRPL) spectroscopy. The TA results show two photoinduced absorption signals at 420 nm and 461 nm and a photoinduced bleach (PB) signal at 448 nm. The PB recovery signal was fitted with a triple exponential function with fast (7.6 ps), medium (43 ps), and slow (450 ps) time constants. The fast component is attributed to vibrational relaxation within the initial excited state and the medium component to shallow carrier trapping. The slow component is attributed to deep carrier trapping from the initial conduction band edge and shallow trap state. The TRPL shows longer timescale kinetics with time constants of 6 and 30 ns attributing to recombination through the deep trap state and direct band edge recombination. The significant role of exciton trapping processes in the dynamics indicates these highly confined nanoclusters have defect-rich surfaces.

TOC Graphic
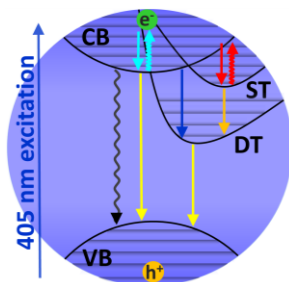
Perovskite nanoclusters (PNCLs) are a class of quasi-crystalline semiconductor nanoclusters with strong quantum confinement and a discrete size or narrow size distribution.[1–3] PNCLs act as stable building blocks or intermediates that form before 0D perovskite quantum dots (PQDs) and larger perovskite nanocrystals. They are much smaller than their nanocrystal counterparts, less than 3 nm, and offer a bluer emission window. Investigating PNCLs may illuminate the growth mechanisms of PQDs on a molecular and/or atomic level and assist in the rational design of high-quality PQDs with molecular precision.

PNCLs are ligand passivated and exhibit the ABX_3 perovskite structure (A being a monovalent cation, B being a metal divalent cation, and X being a halide anion) but form a layered, disc-like morphology in comparison to cubic morphology of PQDs.[2] Recent studies have found that the $CH_3NH_3PbBr_3$ PNCL system is quasi-crystalline and forms a distorted orthorhombic structure.[3] Similar to PQDs, PNCLs are expected to exhibit quantum confinement effects due to their close proximity in size to the Bohr radius of $CH_3NH_3PbBr_3$ perovskites, ~2.0 nm.[4] However, PNCLs are much smaller and exhibit energetically blue shifted, characteristic absorption peak around 450 nm, compared to PQDs, which have a characteristic broad absorption band with an onset around 520 nm.[5] The absorption band of PNCLs indicates a narrower size distribution in

comparison to more polydisperse PQDs. The polydispersity of PQDs after synthesis is likely due to a mixture of these PNCLs and other synthetic intermediate clusters.

Another related intermediate cluster is metal halide molecular clusters (MHMC) that can form during PNCL and PQD synthesis. Ligand-passivated MHMCs lack the A component in perovskite yet still form octahedrally coordinated Pb-Br polyhedra structures similar to the $PbBr_6$ octahedra formed in perovskite.[6] The PNCLs are likely formed from the MHMC intermediate cluster and may retain some MHMC optical characteristics. Although much work has been done optimizing synthesis and characterizing the optical and structural properties of PNCLs, there has yet to be a kinetic study on the exciton dynamics.[1–3]

Studying the exciton dynamics will give us insight into the role defects play in the optoelectronic properties of these novel nanoclusters. For instance, internal or surface defects strongly affect photoluminescence quantum yield (PLQY). Defects are often significant in nanocrystals compared to bulk materials due to their large surface to volume ratio. In smaller PQDs, incomplete surface passivation due to steric hindrance of the ligands can introduce more surface defects.[7] From a kinetics perspective, the high density of surface defect states can contribute to trapping and nonradiative recombination of excitons, thereby lowering the PLQY.[8] PNCLs have a much larger surface to volume ratio than their PQD counterparts, making them a suitable model system for studying the effects of surfaces or interfaces on exciton dynamics.

Surface defects are known to generate trap states within the bandgap which allow for alternate radiative and nonradiative exciton recombination pathways. Shallow trap states, located near the band edges, coupled with low phonon energies lead to low non-radiative recombination rates and thus long carrier lifetimes.[9] This manifests as broadening of the steady-state optical absorption and emission spectra. Deep trap states, located near the middle of the bandgap, generate

non-radiative recombination pathways that can significantly reduce PLQY due to multi-phonon recombination processes.[10]

Herein, this study utilizes femtosecond transient absorption spectroscopy (TA) and time-correlated single photon counting or time-resolved photoluminescence (TRPL) to probe the exciton properties of PNCLs. The results help to clarify the key kinetic processes involved in the exciton dynamics of the PNCL.

Hot ligand assisted reprecipitation was used to synthesize stable PNCL suspensions in toluene.[5] This synthetic method at elevated temperatures was selected because room temperature ligand-assisted reprecipitation synthesis typically shows signs of degradation after several days. PNCLs synthesized with hot ligand-assisted reprecipitation are stable for about a week in ambient conditions, which is necessary for laser operation to carry out the exciton dynamics studies.
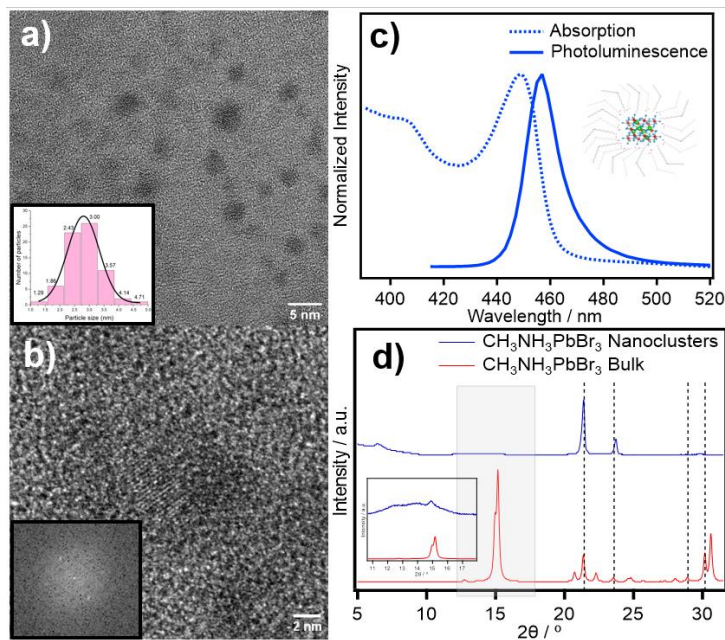
Figure 1 a) HR-TEM of PNCLs illustrating monodispersed particle size histogram (inset), b) HR-TEM of single PNCL showing distorted orthorhombic crystal structure and fast Fourier transform (inset), c) absorption and photoluminescence spectrum of $CH_3NH_3PbBr_3$ PNCL suspended in toluene. Spectrums overlaid and normalized to the corresponding peak absorption and emission. The inset shows the orthorhombic structure of $CH_3NH_3PbBr_3$ PNCL composed of $CH_3NH_3^+$ (green); Pb^{2+} (red); Br^- (blue) passivated with oleic acid and oleylamine ligands (structure constructed using VESTA (COD ID: 4510745))[11] d) X-ray diffraction of distorted orthorhombic $CH_3NH_3PbBr_3$ PNCL with theoretical orthorhombic powder patterns were calculated in VESTA (ICSD: 158306).

Figure 1a shows the high-resolution electron microscopy (HR-TEM) images of PNCLs displaying a relatively monodisperse size distribution. The nanoclusters have an average diameter of 2.8 ± 0.5 nm and a root mean squared of 22%. Figure 1b shows a single PNCL with the fast Fourier transform in the inset. There is likely some error associated with the HR-TEM results due to PNCL instability as a solid. PNCLs tend to aggregate and create larger PQDs when dried to a solid. To avoid this aggregation for powder X-ray diffraction (XRD) measurements, the PNCLs were suspended and stabilized in paraffin as previously reported in literature.[3] Figure 1d shows the powder XRD with the theoretical orthorhombic $CH_3NH_3PbBr_3$ patterns. The HR-TEM shows a d-spacing of ~0.6 nm which agrees with the theoretical $CH_3NH_3PbBr_3$ 14.9° XRD peak in Figure 1d. This result shows that PNCLs have a distorted orthorhombic structure and agrees with previously reported HR-TEM and XRD.[3]

Figure 1c shows the normalized absorption and steady-state photoluminescence (PL) of the PNCL suspensions. The Figure 1c inset illustrates the orthorhombic structured PNCL with oleic acid and oleylamine passivating ligands. The UV-Vis absorption spectrum exhibits an excitonic

absorption peak at 449 nm, while the PL spectrum shows a single emission peak at 457 nm with a full-width half maximum (FWHM) of 19 nm. The PNCLs have a relatively large Stokes shift of 8 nm in comparison to the traditional PQDs that usually have a negligible Stokes shift. A larger Stokes shift has been observed in more confined structures and attributed to a confined hole state associated with defects.[12]

The steady-state absorption and PL show well defined transitions and the strongly confined system suggests that excitonic species are forming. The single, narrow absorption band and narrow FWHM of the PL are characteristic of PNCLs due to their narrow size distribution. Figure S1 shows the PL spectrum best fits with a double Gaussian function, with fitting parameters summarized in Table S1. The inhomogeneous broadening observed in the PL suggests the possibility of two different particle size populations, the presence of defects, or phonon broadening.[13] The photoluminescence excitation spectrum (PLE) in Figure S2 was taken at the peak locations in the fitted PL spectrum (456 and 465 nm). The PLE shows both emissions originate from the same peak at 447 nm which agrees with the first excitonic absorption. This suggests that the photoluminescence originates from the same particle population. In addition, Figure S3 shows wavelength-dependent TRPL with 405 nm excitation was also taken on the two fitted peak locations. Table S2 shows the single-wavelength fitting parameters. There were no changes in the kinetics indicating the photoluminescence originates from the same particle population. It was anticipated that the inhomogeneous broadening may indicate the presence of defects or phonon broadening.

Femtosecond TA studies of PNCLs were conducted by exciting above the band edge at 405 nm and probing with broadband white light in the range of 410-850 nm as a function of the time delay between the pump and probe pulses. The time delay ranged from -2 to 2480 ps to

capture the kinetic decay profile. Kinetic decays provide useful information to model the exciton dynamics, but it is critical to consider power dependent kinetics.

As observed in analogous PQDs, TA analysis can be challenging due to overlapping signals from photoinduced absorption (PA) signals, hot carrier cooling, and stimulated emission, especially at high excitation powers.[8,14,15] In addition, nonlinear processes like Auger recombination and/or exciton-exciton annihilation can also overlap with the signal.[8,16] Thus, power dependent studies were conducted with the goal of finding the threshold excitation power below which nonlinear processes have no effect.
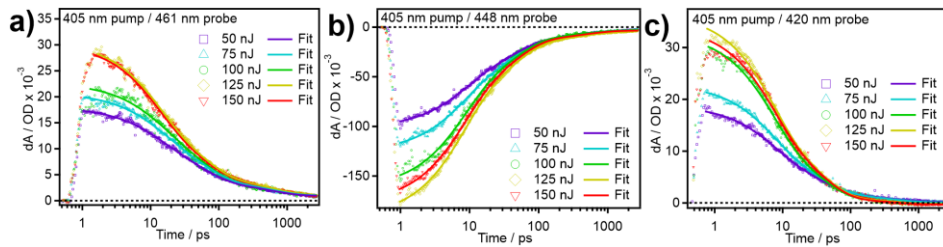

Figure 2 Power dependent kinetic decay profiles of PNCLs excited with 405 nm at different probe signals a) 420 nm probe (PA_1) b) 448 nm probe (PB) and c) 461 nm probe (PA_2). Probe signals are single-wavelengths with the highest dA intensity in the difference in absorption spectrum in Figure 3a.

Figure 2a-c shows the kinetic decay profile at different powers for each photoinduced signal. To identify the threshold power, the PNCL sample was pumped with several pulse energies: 50, 75, 100, 125, and 150 nJ/cm^2. The photoinduced transient signals, or monitored wavelengths at maximum intensity, were determined from the difference in absorption spectrum plotted in Figure 3a. There are two photoinduced absorption features, labeled as PA_1 and PA_2 for the peak position at 420 and 461 nm, and a photoinduced bleach (labeled PB) signal peaked at 448 nm.

Each single-wavelength probe signal was normalized and best fitted with a triple exponential function to determine the decay time constants (τ_x, in ps) and relative amplitudes (A_x, %), where x is the corresponding fitted exponential decay. The corresponding fitting parameters and average decay times for the PA/PB signals are reported in Table S3. The calculated average decay times of the three probe signals, PA_1, PB, and PA_2, were calculated using Equation S1. The respective time constants of each PA or PB feature remained consistent over the different excitation powers used, suggesting invariable kinetics within 50-150 nJ/cm^2 excitation range. However, starting at 100 nJ/cm^2, the amplitude of the observed features lose their linearity suggesting non-linear effects and/or a recombination/excitation bottleneck. Figure S4 shows the amplitude evolution of each signal as a function of power. As observed in smaller PQD systems, highly confined excitons within a single particle limit direct band edge recombination resulting in power-independent decay dynamics.[7,17] This phenomenon is likely occurring in PNCLs which are smaller and more confined and may absorb fewer photons per pulse in comparison to larger nanoparticles like PQDs. To avoid non-linear kinetics and/or an excitation bottleneck, the data from the 50 nJ/cm^2 excitation was used for the exciton dynamic study and kinetic model.
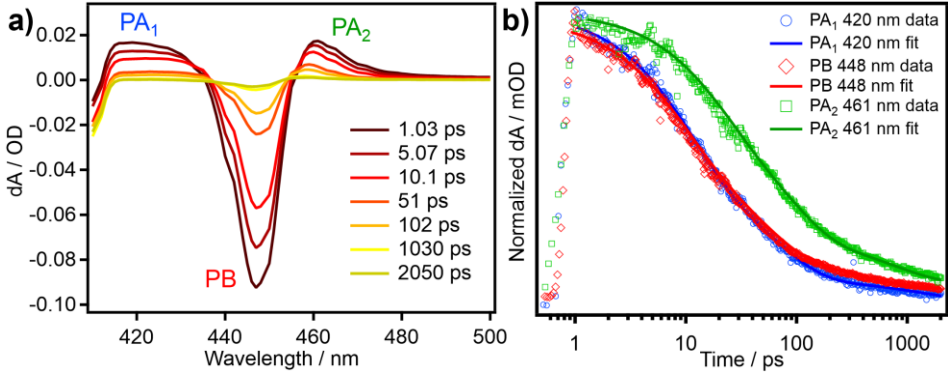
Figure 3 a) Difference in absorption spectrum as a function of wavelength and varying probe delay times and b) Overlaid kinetic decay profiles of the PB and PA_2 signals. Femtosecond TA of PNCLs suspended in toluene were collected by exciting samples at 405 nm (above the band edge) probing with an ultraviolet white light continuum (350−600 nm) as a function of time delay between the pump and probe pulses.

The 420 nm PA_1 decay profile can be fit with a triple exponential with a fast, medium, and slow time constant of 6.6 ± 0.5, 36 ± 5, and 370 ± 50 ps. The PB signal, albeit with opposite signs, can be fit with similar time constants. Figure 3b shows the overlaid PA_1, PB, and PA_2 kinetic decays to confirm kinetic agreement. In addition, Figure S5 shows box plots comparing the fast, medium, and slow time constants of each corresponding TA signal. The similar kinetics of the PA_1 and PB signal suggest that they are associated with the same dynamics. The initial positive absorption feature of PA_1 is attributed to electrons excited to the first excitonic state or conduction band (CB). The decay profile of the PA_1 feature reflects the dynamics of the photogenerated electrons in the CB, which seem to match the dynamics of the PB reflecting recovery of the electrons back in the valence band (VB). The 461 nm PA_2 feature shows generally longer kinetics compared to the PB or PA_1. The PA_2 kinetics show fast, medium, and slow time constants of 11.3 ± 0.8, 55 ± 4, and 580 ± 70 ps. The overlaid kinetic decay profiles in Figure 3b and the time constant comparisons in Figure S5 show that the PA_2 feature has a slow decay unique to the PNCLs. This slower decay may be attributed to trap states absorbing the 461 nm probe.

The 448 nm PB decay profile is attributed to the repopulation of ground state electrons due to the good agreement with the first excitonic absorption in the UV-Vis spectrum shown in Figure 1c. The PB decay profile was best fit with a triple exponential with fast (7.6 ± 0.5 ps),

medium (43 ± 3 ps), and slow (450 ± 40 ps) decay time constant. The decay profile was

normalized to obtain the relative amplitudes as percentages of each decay time component.

Relative amplitudes were used to indicate the dominant processes contributing to the bleach

recovery. The fast and medium time components have large amplitudes, $46 \pm 1\%$ for A_1 and $40 \pm$

1% for A_2, suggesting these are the dominant processes occurring in bleach recovery. The slow

time component has an amplitude of $10.4 \pm 0.5\%$ (A_3) indicating a minor process contributing to

the bleach recovery. Although the PB decay profile provides information on ultrafast

recombination kinetics, it is an incomplete picture of the kinetics on longer time scales because

the PB signal was not fully recovered within the time window (2480 ps). TRPL was conducted to

map out the long-time scale recombination kinetics to the nanosecond regime.

Commented [FB1]: Is there a reason to not use the microsecond TA system for this?

Figure 4 shows the PL decay profile of PNCLs excited above the band edge at 405 nm

and the emission was collected at 454 nm. The PL decay was best fit using a double exponential

function, and the fitting parameters and average PL decay time are reported in Table S4. The PL

decay profile of the PNCLs revealed a fast (6.0 ± 0.2 ns) and slow (28.6 ± 0.2 ps) decay time

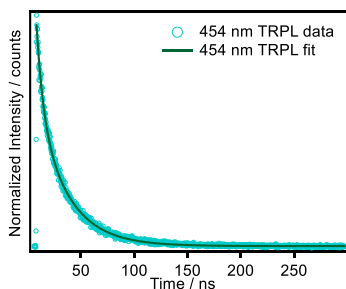constant. The average PL decay lifetime was calculated, using Equation S1, to be 26 ps.

Figure 4 Time-resolved photoluminescence of PNCLs excited at 405 nm. Monochromator wavelengths set at λ_{max}= 454 nm emission.

The fast and slow components have relative amplitudes of $33.8 \pm 0.5\%$ and $61.0 \pm 0.5\%$ suggesting the competitive nature of the two processes contributing to the observed decay in PL. This indicates the presence of a trap state within the band gap that is facilitating a competitive emission pathway to drive faster band edge recombination. The fast 6 ns component was contributed to the electron-hole recombination through a trap state and the slow 28.6 ns component is consistent with direct band edge recombination.[7] A power dependent study was conducted to determine the saturation of the trap states in Figure S6. However, there is no trend in the power dependence and the kinetic is unchanging.

Radiative and nonradiative recombination lifetimes were found using the TRPL and relative PLQY (28% compared against a perylene/cyclohexane reference) to determine dominant

11

Commented [VLC2]: Not sure what to conclude here

Commented [FB3R2]: Yeah, Fig 6b looks a bit wierd

decay processes. The PLQY provides a measure of the radiative versus nonradiative processes. The relationship between observed PL lifetime (τ_{obs}), radiative lifetime (τ_r), and PLQY is shown in Eq. 1.[18]

$$\tau_r = \frac{\tau_{obs}}{PLQY} \qquad (1)$$

The radiative and nonradiative lifetimes were calculated using Eq. 2[18],

$$\frac{1}{\tau_{obs}} = \frac{1}{\tau_r} + \frac{1}{\tau_{nr}} \qquad (2)$$

where (τ_{obs}), (τ_r), and (τ_{nr}) are the average PL lifetime, radiative lifetime, and nonradiative lifetime. Using the average observed average lifetime (26 ns) and the measured PLQY (28 %) of PNCLs, τ_r and τ_{nr} were calculated to be 93 and 37 ns, respectively. The radiative lifetime is over 2 times longer than the nonradiative lifetime indicating the dynamics are dominated by the nonradiative processes. Unlike PQD samples where radiative processes are dominant, PNCLs are similar to MHMC samples, where nonradiative processes are dominant suggesting the presences of defect-related recombination.

The TA and TRPL results were used to construct a kinetic model and propose the possible recombination processes occurring in PNCLs. Figure S7 shows the overlaid TA and TRPL kinetic decay profiles and full kinetic fit to confirm the decay lifetimes. Kinetic modeling using the full decay profile from the experimental TA and TRPL data was used to construct a simple mechanism to aid in explaining the possible relaxation processes involved in these novel clusters. Details of the kinetic modeling are available in Supporting Information: Figures S8-S10, Table S5, and Equations S2-S6.

Figure 5 shows a proposed kinetic model for the exciton dynamics of PNCLs with a focus on key processes under low excitation power where nonlinear processes that tend to occur

at high excitation power are less likely due to their nature. The proposed exciton processes involve the CB, CB edge (CB$_{edge}$), shallow trap (ST) states, deep trap (DT) states, and VB. An exciton is generated after excitation with energy above the band gap. Exciting above the band edge provides excess kinetic energy and, therefore, the electron will relax to the CB$_{edge}$ through electron−phonon interactions.[15]
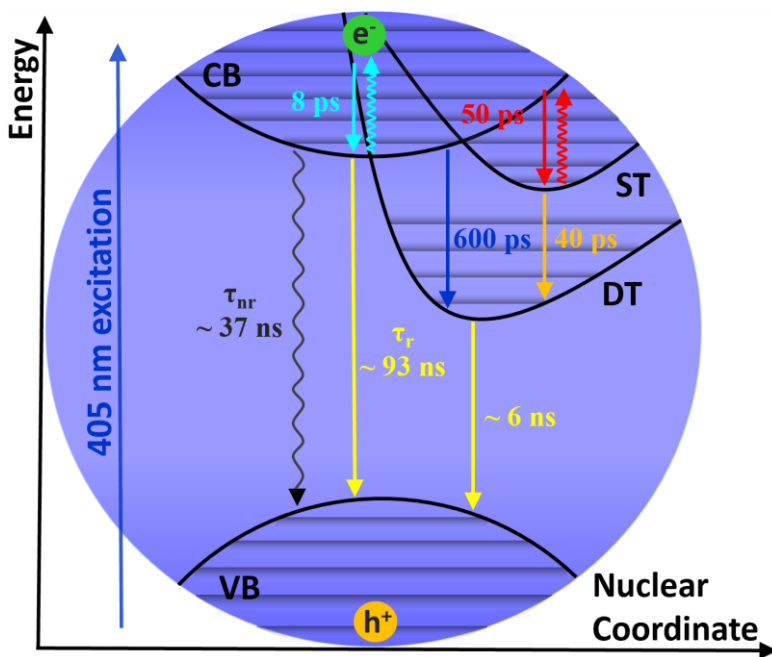

Figure 5 Kinetic model of PNCL. Lifetimes of each state were estimated using decay time constants found in the TA and TRPL results.

The fast component (~8 ps) in the PB decay profile was attributed to vibrational relaxation or cooling of the excitons within the CB. In MHMC systems, vibrational relaxation has a similar ultrafast decay lifetime of ~7 ps, which suggests that PNCLs have some MHMC

character.[19] After the electrons have relaxed to the CB_{edge}, they can go through multiple pathways, including trapping into trap states. The Urbach absorption tail seen in PNCLs, also seen in semiconductor nanocrystals, is known to be due to localized energy states (shallow trap/defect sites) near the band-edge arising from the structural disorder or lattice defects.[20,21] In addition, the triple exponential decay of the PB signal indicates that the dynamic processes are not simple sequential or parallel processes but reverse processes.[7,22] The possible reverse processes are shown in Figure 5 as upward curved arrows. The reverse processes are usually expected to be slower than the forward process.[7] The reverse process is likely due to back energy transfer from vibrationally relaxed states within the CB or trap states to higher vibrational states resulting in multiexponential character. The respective rate constants and associated time constants are displayed in Table S5. Multiple combinations of rate constants and time constants were simulated to troubleshoot the most plausible processes occurring within the PNCL system.

In the simplified model, it was found that the PB medium component (~50 ps) was attributed to shallow trapping below to CB. It was also found that the CB and ST states were also coupled to a DT state (40 and 600 ps) and both forward processes were contributing to deep trapping. However, each of these ultrafast processes did not contribute to overall observed PL lifetime.

In PNCLs, the relaxed electron can recombine radiatively, resulting in PL, or non-radiatively with the hole in the electronic ground state. The dominant recombination pathway is through direct band edge recombination giving a radiative lifetime of ~93 ns and a nonradiative lifetime of ~37 ns. However, the electron may also recombine through deep trapping as well. The fast decay lifetime (~6 ns) in the TRPL may be from trapping in a DT state. Figure S3 and Table

14

S2 shows wavelength-dependent TRPL to confirm the presence of deep trapping. We found that the fast component of the TRPL (or slow component of the PB) increased in amplitude when the monochromator was centered at 465 nm (below the band edge). This indicates an increase in population of a low energy state below the band edge causing deep trapping.

> **Commented [VC4]:** Is this a correct interpretation?
>
> **Commented [VLC5R4]:** This was for 330 nm excitation

The proposed PNCL kinetic model suggests that the dominant processes in the PB kinetics are vibrational relaxation to CB and shallow trapping of electrons. The PB kinetics reveal a minor recombination pathway identified by the (~6 ns). Recombination through the deep trap state is a minor emission pathway. The slow component of the TRPL (~29 ns) is then attributed to the direct band edge emission and is the dominant emissive recombination pathway. The high density of trap states suggests that PNCLs have a defect rich surface. Smaller nanocrystals tend to have a higher density of defects due to a larger surface to volume ratio and less effective surface passivation due to steric hindrance caused by a relatively bulky capping ligand in proportion to the size of the nanocrystal.

In summary, the exciton dynamics of methylammonium lead halide NCLs have been investigated for the first time using femtosecond TA spectroscopy and TRPL. The fast and medium components in the PB kinetics were found to be the dominant processes, indicating vibrational relaxation in the excited state and shallow trapping plays a significant role in recombination. The deep trap state provides an alternate pathway for recombination. Although trap-assisted recombination processes occur in NCLs, direct band edge recombination is still dominant showing that PNCLs are defect tolerant like their perovskite counterparts. The surface defects in PNCLs may be causing exciton trapping and contribute to overall shorter lifetimes in comparison to PQDs.

Associated Content

Supporting Information

Author Information

Corresponding Authors

*E-mail: zhang@ucsc.edu

Notes

The authors declare no competing financial interest.

Commented [FB6]: The foundry websites states this phrasing: *Work at the Molecular Foundry was supported by the Office of Science, Office of Basic Energy Sciences, of the U.S. Department of Energy under Contract No. DE-AC02-05CH11231.*

In any case I would propose to include the doe funding number

In case you measured TEM (and the data is conclusive/good) I would include it in the SI

References

(1) Vickers, E. T.; Chen, Z.; Cherrette, V.; Smart, T.; Zhang, P.; Ping, Y.; Zhang, J. Z. Interplay between Perovskite Magic-Sized Clusters and Amino Lead Halide Molecular Clusters. *Research* **2021**, *2021*, 2021/6047971. https://doi.org/10.34133/2021/6047971.

(2) Zhang, B.; Altamura, D.; Caliandro, R.; Giannini, C.; Peng, L.; De Trizio, L.; Manna, L. Stable CsPbBr$_3$ Nanoclusters Feature a Disk-like Shape and a Distorted Orthorhombic Structure. *J. Am. Chem. Soc.* **2022**, *144* (11), 5059–5066. https://doi.org/10.1021/jacs.1c13544.

(3) Guarino-Hotz, M.; Barnett, J. L.; Chou, K.-C.; Win, A. A.; Zhang, H.; Song, C.; Oliver, S. R. J.; Zhang, J. Z. Structural Study of Paraffin-Stabilized Methylammonium Lead Bromide

Magic-Sized Clusters. *J. Phys. Chem. C* **2023**, *127* (6), 3367–3376. https://doi.org/10.1021/acs.jpcc.2c08645.

(4) Tanaka, K.; Takahashi, T.; Ban, T.; Kondo, T.; Uchida, K.; Miura, N. Comparative Study on the Excitons in Lead-Halide-Based Perovskite-Type Crystals CH3NH3PbBr3 CH3NH3PbI3. *Solid State Communications* **2003**, *127* (9–10), 619–623. https://doi.org/10.1016/S0038-1098(03)00566-0.

(5) Guarino-Hotz, M.; Barnett, J. L.; Pham, L. B.; Win, A. A.; Cherrette, V. L.; Zhang, J. Z. Tuning between Methylammonium Lead Bromide Perovskite Magic-Sized Clusters and Quantum Dots through Ligand Assisted Reprecipitation at Elevated Temperatures. *J. Phys. Chem. C* **2022**, *126* (32), 13854–13862. https://doi.org/10.1021/acs.jpcc.2c04384.

(6) Zhang, H.; Vickers, E. T.; Erickson, S.; Guarino-Hotz, M.; Barnett, J. L.; Ghosh, S.; Zhang, J. Z. Synthesis and Properties of Stable Amino Metal Halide Molecular Clusters in the Solid State. *J. Phys. Chem. Lett.* **2022**, *13* (45), 10543–10549. https://doi.org/10.1021/acs.jpclett.2c02977.

(7) Naghadeh, S. B.; Luo, B.; Pu, Y.-C.; Schwartz, Z.; Hollingsworth, W. R.; Lindley, S. A.; Brewer, A. S.; Ayzner, A. L.; Zhang, J. Z. Size Dependence of Charge Carrier Dynamics in Organometal Halide Perovskite Nanocrystals: Deciphering Radiative Versus Nonradiative Components. *J. Phys. Chem. C* **2019**, *123* (7), 4610–4619. https://doi.org/10.1021/acs.jpcc.9b00711.

(8) Luo, B.; Pu, Y.-C.; Yang, Y.; Lindley, S. A.; Abdelmageed, G.; Ashry, H.; Li, Y.; Li, X.; Zhang, J. Z. Synthesis, Optical Properties, and Exciton Dynamics of Organolead Bromide Perovskite Nanocrystals. *J. Phys. Chem. C* **2015**, *119* (47), 26672–26682. https://doi.org/10.1021/acs.jpcc.5b08537.

(9) Kirchartz, T.; Markvart, T.; Rau, U.; Egger, D. A. Impact of Small Phonon Energies on the Charge-Carrier Lifetimes in Metal-Halide Perovskites. *J. Phys. Chem. Lett.* **2018**, *9* (5), 939–946. https://doi.org/10.1021/acs.jpclett.7b03414.

(10) Toyozawa, Y. Multiphonon Recombination Processes. *Solid-State Electronics* **1978**, *21* (11–12), 1313–1318. https://doi.org/10.1016/0038-1101(78)90199-5.

(11) Koichi Momma; Fujio Izumi. VESTA, 2011.

(12) Brennan, M. C.; Kuno, M.; Rouvimov, S. Crystal Structure of Individual CsPbBr₃ Perovskite Nanocubes. *Inorg. Chem.* **2019**, *58* (2), 1555–1560. https://doi.org/10.1021/acs.inorgchem.8b03078.

(13) Cherrette, V. L.; Babbe, F.; Cooper, J. K.; Zhang, J. Z. Octahedral Distortions Generate a Thermally Activated Phonon-Assisted Radiative Recombination Pathway in Cubic CsPbBr₃ Perovskite Quantum Dots. *J. Phys. Chem. Lett.* **2023**, *14* (39), 8717–8725. https://doi.org/10.1021/acs.jpclett.3c02568.

(14) Manser, J. S.; Christians, J. A.; Kamat, P. V. Intriguing Optoelectronic Properties of Metal Halide Perovskites. *Chem. Rev.* **2016**, *116* (21), 12956–13008. https://doi.org/10.1021/acs.chemrev.6b00136.

(15) Fu, J.; Xu, Q.; Han, G.; Wu, B.; Huan, C. H. A.; Leek, M. L.; Sum, T. C. Hot Carrier Cooling Mechanisms in Halide Perovskites. *Nat Commun* **2017**, *8* (1), 1300. https://doi.org/10.1038/s41467-017-01360-3.

(16) Roberti, T. W.; Cherepy, N. J.; Zhang, J. Z. Nature of the Power-Dependent Ultrafast Relaxation Process of Photoexcited Charge Carriers in II-VI Semiconductor Quantum Dots: Effects of Particle Size, Surface, and Electronic Structure. *The Journal of Chemical Physics* **1998**, *108* (5), 2143–2151. https://doi.org/10.1063/1.475593.

(17) Wheeler, D. A.; Fitzmorris, B. C.; Zhao, H.; Ma, D.; Zhang, J. Ultrafast Exciton Relaxation Dynamics of PbS and Core/Shell PbS/CdS Quantum Dots. *Sci. China Chem.* **2011**, *54* (12), 2009–2015. https://doi.org/10.1007/s11426-011-4407-7.

(18) Zhang, J. Z. *Optical Properties and Spectroscopy of Nanomaterials*; WORLD SCIENTIFIC, 2009. https://doi.org/10.1142/7093.

(19) Zhang, H.; Zeitz, D. C.; Zhang, J. Z. Ultrafast Study of Excited State Dynamics of Amino Metal Halide Molecular Clusters. *J. Phys. Chem. Lett.* **2023**, *14* (36), 8095–8099. https://doi.org/10.1021/acs.jpclett.3c01952.

(20) Mondal, N.; Samanta, A. Complete Ultrafast Charge Carrier Dynamics in Photo-Excited All-Inorganic Perovskite Nanocrystals (CsPbX$_3$). *Nanoscale* **2017**, *9* (5), 1878–1885. https://doi.org/10.1039/C6NR09422H.

(21) Sheng, C.; Zhang, C.; Zhai, Y.; Mielczarek, K.; Wang, W.; Ma, W.; Zakhidov, A.; Vardeny, Z. V. Exciton versus Free Carrier Photogeneration in Organometal Trihalide Perovskites Probed by Broadband Ultrafast Polarization Memory Dynamics. *Phys. Rev. Lett.* **2015**, *114* (11), 116601. https://doi.org/10.1103/PhysRevLett.114.116601.

(22) Pu, Y.-C.; Kibria, M. G.; Mi, Z.; Zhang, J. Z. Ultrafast Exciton Dynamics in InGaN/GaN and Rh/Cr$_2$O$_3$ Nanoparticle-Decorated InGaN/GaN Nanowires. *J. Phys. Chem. Lett.* **2015**, *6* (13), 2649–2656. https://doi.org/10.1021/acs.jpclett.5b00909.